LQG/LTR Control of an AC Induction Servo Drive

Ying-Yu Tzou, *Member, IEEE,* and Hsiang-Jui Wu

***Abstract*—A new design method based on the linear-quadratic-Gaussian with loop-transfer-recovery (LQG/LTR) theory has been developed for the design of high performance ac induction servo drives using microcomputer-based digital control. The principle of field orientation is employed to achieve the current decoupling control of an induction motor. An equivalent model representing the dynamics of the decoupled induction motor has been developed. Based on the developed model with specified parameter uncertainties and given performance specifications, a frequency domain loop-gain-shaping method based on the LQG/LTR theory is proposed for the design of the servo loop controller. A microcomputer-based induction servo drive has been constructed to verify the proposed control scheme. Simulation and experimental results are given to illustrate the effectiveness of the proposed design method.**

NOMENCLATURE

P	Number of poles.
R_s, R_r	Stator and rotor resistances.
L_s, L_r	Stator and rotor inductances.
L_m	Mutual magnetizing inductance.
i_{qs}, i_{ds}	Torque and flux-producing currents.
i_{mr}	Magnetizing current.
ψ_r	Rotor flux.
T_e	Motor developed electrical torque.
T_d	Load disturbance torque.
J_m	Lumped inertia.
B_m	Viscous constant.
ω_e	Synchronous angular velocity.
ω_r	Rotor electrical angular velocity $((P/2)\omega_m)$.
ω_m	Rotor mechanical angular velocity.
ω_{sl}	Slip angular velocity.
ω_r	Rotor flux angular position.
ω_m	Rotor angular position.
τ_r	Rotor time constant (L_r/R_r).
τ_e	Electrical time constant.
τ_m	Mechanical time constant.
K_I	Current control gain.
K_T	Motor equivalent torque constant.
K_E	Motor equivalent voltage constant.

I. INTRODUCTION

An ac induction motor as a controlled plant has a nonlinear and highly interacting multivariable structure which can be described by a set of nonlinear differential equations. The analysis and control problem with such complicated dynamic properties has been overcome by using the principle of field orientation [1] which reduces the control of an ac induction motor to that of a separately excited dc motor. Because of the intense advances of microelectronics and power electronics, inverter-fed ac induction servo drives controlled by the field orientation strategy and linear control system design methodology are becoming dominant in many applications where fast and precision operation is required [2], [3].

Due to the fast development in automation technology, the demand for high performance electrical servos has been increasing. To achieve precision operation and meet the high performance servo requirements, it is necessary to develop a controller that overcomes the influence of parameter variations, plant uncertainties, and load disturbances. The design of controller that guarantee performance and stability robustness has become an important issue in current servomechanism systems [4]. A number of approaches have been introduced in the synthesis of a robust controller. But no matter how powerful the methodology is, a typical application requires several iterations. Therefore, it is imperative that the design procedures are transparent and conductive to educated trial and error design iterations, and the number of design parameters should keep at a minimum. The linear-quadratic-Gaussian with loop-transfer-recovery (LQG/LTR) methodology [5] has many of the required characteristics of an easy-to-use design method for SISO and MIMO feedback control. The LQG/LTR design procedure merges the LQG optimal control problem with the robust recovery procedure that recovers the desired robustness properties associated with the linear-quadratic-regulator (LQR) design. Extensive descriptions and applications of the LQG/LTR methodology can be found in [6]–[9]. Using the LQG/LTR methodology, the control system loop transfer function can be shaped so that the closed-loop system will yield 1) good command following, 2) good output disturbance rejection, and 3) good robustness (insensitivity) to noises and unmodeled system dynamics. In this paper, the LQG/LTR methodology is applied to the design of the servo loop controller of an ac induction servo drive using a 16-bit microprocessor Intel 80486. The proposed LQG/LTR control scheme can improve the drive dynamic performances and meet the stability-robustness requirement according to given frequency response specifications.

The remainder of this paper is organized as follows. Section II describes the modeling process. An equivalent model of the induction servo motor under indirect field-oriented feedforward vector control employing current-controlled PWM inverter is derived. Section III presents the proposed LQG/LTR

Manuscript received June 3, 1993; revised October 3, 1994. This work was supported by National Science Council, Taipei, Taiwan, ROC, under Project NSC80-0404-E009-46.

The authors are with Power Electronics & Motion Control Lab., Institute of Control Engineering, National Chiao Tung University, Hsinchu 300 Taiwan, ROC.

IEEE Log Number 9408511.

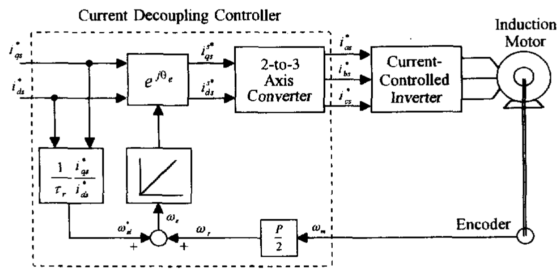

Fig. 1. Current decoupling control of an ac induction motor.

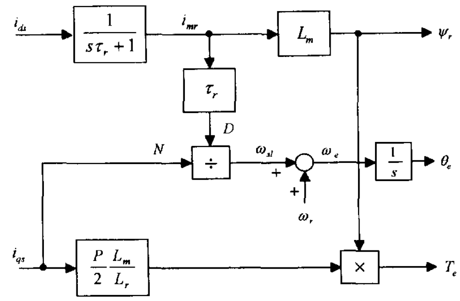

Fig. 2. Rotor flux model in field coordinates.

controller design procedure. The mathematical model developed in the previous section is used as nominal model to illustrate the controller design procedure. The derived LQG/LTR compensator can be easily applied to the complete model when the drive operating in full control range. However, the nominal plant model does not capture all the relevant high frequency dynamics of the physical controlled plant. The modeling errors and plant uncertainties have been estimated in the frequency domain and imposed stability-robustness specification. According to the design specifications a target feedback loop is developed to meet the performance and stability-robustness requirements. The augmented dynamics and weighting functions associated with the LQG/LTR design are also shown in this section. Implementation of the proposed servo controller and experimental results are presented in Section IV. A prototype of 80486-based ac induction servo drive system has been implemented and used to evaluate the proposed design approach. Experimental results have shown the applicability of the LQG/LTR control theory in the design of an ac induction servo drive. Conclusions are given in Section V.

II. Decoupling Control and Modeling

Investigating the approaches for field-oriented control system, the feedforward indirect control method [10] has been widely discussed because it offers the advantage of nondectection of the rotor flux and even the stator currents. This method uses a feedforward loop to estimate the position of the rotor flux via an algebraic operation on the stator current component references and the rotor angular frequency. The feedforward indirect field orientation is employed to construct the fast response decoupling controller for an ac induction servo as shown in Fig. 1. The decoupling controller associated with the current-controlled PWM inverter results in the current decoupling control operation of an ac induction motor.

Using the decoupling controller, the stator input current vector can be decoupled into two orthogonal current components, the flux-producing current i_{ds} and the torque-producing current i_{qs}. The control action takes place in field coordinates which use the rotating rotor flux vector as a frame of reference. The rotor flux vector referred to the stator is calculated from the stator current components according to the transformed rotor flux model of an ac induction motor shown as Fig. 2.

When the d-axis is fixed on the synchronously rotating rotor flux vector, dynamic equations of a symmetrical induction motor under vector control can be derived based on the d-q two-axis theory and field orientation as

$$i_{\mathrm{ds}} = \tau_r \frac{di_{mr}}{dt} + i_{mr} \tag{1}$$

$$i_{\mathrm{qs}} = (\omega_e - \omega_r)\tau_r i_{mr} = \omega_{\mathrm{sl}}\tau_r i_{mr} \tag{2}$$

$$T_e = \left(\frac{P}{2}\right)\frac{L_m^2}{L_r} i_{mr} i_{\mathrm{qs}} \tag{3}$$

where i_{mr} is the stator-based magnetizing current which produces the rotor flux $\psi_r = L_m i_{mr}$. All symbols are listed in the Nomenclature at the beginning of this paper. The motor developed electrical torque is expressed as (3) which describes the interaction between the torque-producing current and the magnetizing current. When operating in the constant torque region, the magnitude of the magnetizing current is maintained at a maximum level limited by the iron core saturation, while the torque control action is assigned to i_{qs} for fast responses. The current regulation is carried out by using a current-controlled inverter, thus in the stationary reference frame. Since coordinate transformation does not involve any dynamics, the current control action is the same whether in the synchronously rotating or the stationary reference frame. With a negligible current control time constant and for simplicity, a high-bandwidth current feedback loop usually can be represented by an equivalent current loop gain K_I, and the torque-producing current control action can be modeled as

$$\nu_{\mathrm{qs}} = K_I(i_{\mathrm{qs}}^* - i_{\mathrm{qs}}). \tag{4}$$

The magnitude of the magnetizing current as well as the flux-producing current are kept as constants when motor is operating in the constant torque region. The imaginary part of the stator voltage equation in field coordinates can be expressed as

$$\nu_{\mathrm{qs}} = R_s i_{\mathrm{qs}} + \sigma L_s \frac{di_{\mathrm{qs}}}{dt} + L_s \omega_e i_{\mathrm{ds}} \tag{5}$$

where σ stands for the total leakage factor of the motor. Substituting the rotor flux angular frequency ω_e referred to the rotor flux model, (5) becomes

$$\sigma L_s \frac{di_{\mathrm{qs}}}{dt} + R_s i_{\mathrm{qs}} = \nu_{\mathrm{qs}} - \frac{L_s}{L_r} R_r i_{\mathrm{qs}}^* - L_s i_{\mathrm{ds}} \omega_r. \tag{6}$$

The motor dynamics can be expressed as

$$J_m \frac{d\omega_m}{dt} + B_m \omega_m = T_e - T_d. \tag{7}$$

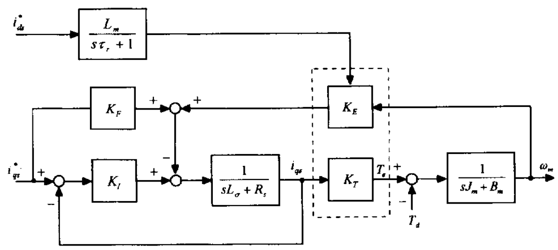

Fig. 3. Equivalent model of a current decoupling controlled induction servo drive.

TABLE I
PARAMETERS OF THE EQUIVALENT MODEL

L_σ	σL_s
σ	$1-\frac{L_m^2}{L_s L_r}$
K_T	$(\frac{P}{2})\frac{L_m}{L_r}(L_m i_{ds})$
K_E	$(\frac{P}{2})\frac{L_s}{L_m}(L_m i_{ds})$
K_F	$(\frac{L_s}{L_r})R_r$

The current decoupling control (6) associated with the mechanical dynamics (7) establish the equivalent model as shown in Fig. 3. It should be noted that not only the ac induction motor but also the inverter current control loop dynamics have been included in the equivalent plant model. The symbols used in the equivalent plant model are listed in Table I.

If the viscous constant is negligible, the equivalent model of the current decoupling controlled ac servo drive can be approximated by a second-order system with the transfer function

$$G_p(s) = \frac{\omega_m(s)}{i_{qs}^*(s)} \tag{8}$$

$$= \frac{(K_I - K_F)K_T}{(L_\sigma J_m)s^2 + (R_s + K_I)J_m s + K_E K_T} \tag{8a}$$

$$= \frac{K'}{(s\tau_e + 1)(s\tau_m + 1)} \tag{8b}$$

where $K' = (K_I - K_F)/K_E$ is the equivalent motor constant, τ_e and τ_m are the equivalent electrical and mechanical time constant, respectively. These parameters can be obtained either via measurements [11] or some kinds of parameter identification techniques [12].

III. LQG/LTR CONTROLLER DESIGN

Fig. 4 shows the proposed servo control scheme for an ac induction motor drive. The design plant model used in conjunction with the LQG/LTR method includes the nominal plant model and the augmented dynamic that appends to the plant model to meet command—following and performance specifications. The transfer function $G(s)$ is used to denote the design plant model

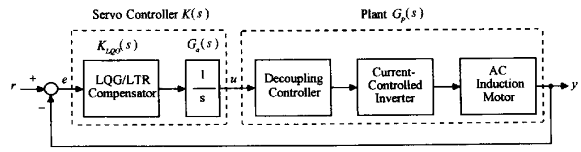

Fig. 4. LQG/LTR servo control scheme of an ac induction motor.

$$G(s) = G_a(s)G_p(s) \tag{9}$$

where $G_p(s)$ stands for the nominal plant model composed by three major parts: the decoupling controller, the current-controlled inverter, and the ac induction motor, and $G_a(s)$ for the augmentation dynamic. In this system $G_a(s)$ is an integrator to achieve integral action due to the zero steady-state error requirement. The overall servo controller $K(s)$ includes the augmented dynamic $G_a(s)$ and the LQG/LTR compensator $K_{\rm LQG}(s)$ as shown in Fig. 4.

The design plant model is imbued in the standard negative identity feedback loop configuration. The impact of all disturbances is accounted for as an equivalent additive disturbance acting on the design plant model output. The LQG/LTR design methodology seeks to define the compensator $K(s)$ so that the stability-robustness and performance specifications are met to the extent possible.

Step 1—Define the Design Plant Model: According to the load and parameter variation ranges as shown in Table II, some extreme test conditions can be made for an ac induction servo drive. Fig. 5 shows the corresponding frequency responses of the plant under various test conditions. Considering the normal operating condition, the nominal plant model is constructed by using the nominal values of load and parameters.

The state space representation of the design plant model is

$$\dot{x}(t) = Ax(t) + Bu(t) + \Gamma\xi(t)$$
$$y(t) = Cx(t) + n(t) \tag{10}$$

where $\xi(t)$ is the process noise and $n(t)$ is the measurement noise. Performance index to be minimized is defined as

$$J = E\left\{\lim_{T\to\infty}\frac{1}{T}\int_0^T \left(y^T y + \rho u^T u\right)dt\right\}. \tag{11}$$

In the canonical form the reduced-order design plant model can be described numerically by the triple (A, B, C) shown in Table III.

Step 2—Determine the Target Feedback Loop: The servo controller is used to allow the motor drive to follow a step command change with no steady-state error and to overcome the plant uncertainties due to large parameter and load variations. These requirements on performance and robustness impose limitations on the loop transfer function and can be interpreted in the frequency domain using the magnitude plot. A target feedback loop is determined in the sense that the target design meets the imposed performance specifications without violating the stability-robustness constraints.

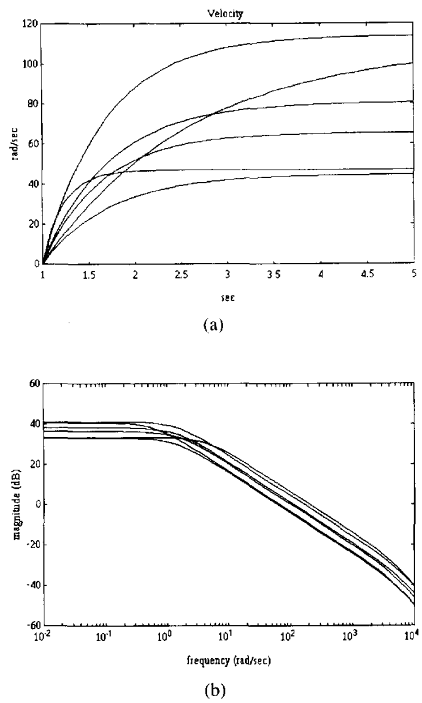

Fig. 5. (a) Time responses. (b) Frequency responses of the decoupled induction motor under parameter and load variations.

TABLE II
PLANT MODEL PARAMETER VARIATIONS

K_I	100	100	V/A
K_E	0.48 ~ 0.59	0.54	V-sec/rad
K_T	0.43 ~ 0.53	0.48	N-m/A
K'	44.7~114	44.7	rad/(sec-A)
τ_e	0.17 ~ 0.19	0.17	msec
τ_m	0.64 ~ 1.6	0.72	sec

TABLE III
NUMERICAL DATA OF THE REDUCED-ORDER DESIGN PLANT MODEL

$$A = \begin{bmatrix} -1.3974 & 0 \\ 1 & 0 \end{bmatrix}$$

$$B = \begin{bmatrix} 1 & 0 \end{bmatrix}^T$$

$$C = \begin{bmatrix} 0 & 62.4 \end{bmatrix}$$

An evaluation concerning the necessary speed loop transfer function is for the positioning servomechanism operation. The position loop gain is designed to be 20 s^{-1}. When a specified distance-to-go positioning command is traversing at a feedrate of 6 m/min, its following error should be less than 5 mm and final position error within $\pm$ 0.001 mm. Under these specifications, Fig. 6 shows the desired step responses of the speed control loop. Fig. 7 illustrates the barriers imposed on the minimum and maximum magnitude values of the loop transfer function to meet these requirements. It is observed that the loop transfer function is required to have at least a 36-dB gain at $\omega = 1$ rad/sec. The system is also required to track command inputs with no steady-state error, thus requiring integral action. A restriction of 200 rad/sec for the maximum crossover frequency of the system is also imposed. For robustness requirements, it is assumed that the plant model is reasonably accurate up to 300 rad/sec, and then uncertainty grows at the rate of 40 dB/decade.

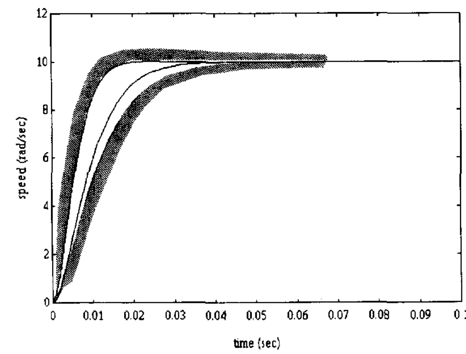

Fig. 6. Desired step responses of the speed control loop.

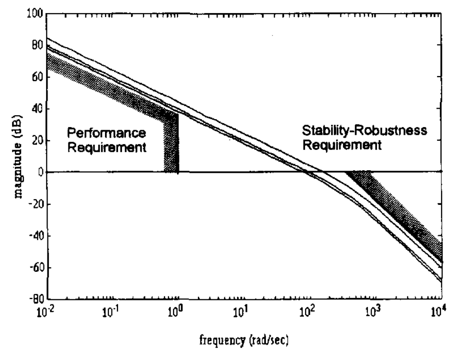

Fig. 7. Performance and stability-robustness barriers.

The Kalman filter technique is then used to design the target feedback loop. Let G_{KF} indicate the target feedback loop transfer function given by

$$G_{\text{KF}}(s) = C(sI - A)^{-1}K_f \tag{12}$$

where K_f is the Kalman filter gain. Process noise $\xi(t)$ is assumed to be white, zero mean, with identity intensity and measurement noise $n(t)$ is assumed to be white, zero mean, and with intensity equal to μ. Solve the filter algebraic Ricatti equation

$$0 = AS + SA^T + \Gamma\Gamma^T - \left(\frac{1}{\mu}\right)SC^TCS. \tag{13}$$

Then the Kalman filter gain is obtained as $K_f = (1/\mu)SC^T$. The desired loop-gain shows a similar shape as an integrator

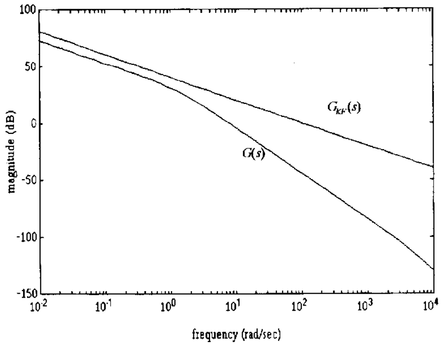

Fig. 8. Magnitude plot of the target feedback loop.

TABLE IV
POLE-ZERO LOCATIONS OF G_{KF} AND K_{LQG}.

G_{KF}	poles:	0	zeros:	-1.535
		-1.397		
K_{LQG}	poles:	-608.8±604.7i	zeros:	-1.535

$1/s$ with gain crossover frequency of 100 rad/sec. This kind of target feedback loop can be synthesized by choosing Γ as

$$\Gamma = \begin{bmatrix} -(CA^{-1}B)^{-1} \\ \alpha C^T(CC^T)^{-1} \end{bmatrix}.$$

In the given design example, $\mu = 0.001$ and $\alpha = 10$ are chosen to achieve the desired closed-loop bandwidth. The Kalman filter gain K_f is obtained as

$$K_f = [0.221 \quad 1.604]^T.$$

The magnitude plot of the target feedback loop transfer function G_{KF} is shown in Fig. 8. The pole-zero locations of G_{KF} are listed in Table IV.

Step 3—Derive the LQG/LTR Compensator: The LQG/LTR compensator belongs to the class of the model-based compensators as illustrated in Fig. 9. The model-based compensator contains a replica of the design plant model together with two feedback loops. One of the feedback loop gains is fixed to be the Kalman filter gain K_f found in Step 2. The other, the control gain K_c, is computed via the solution of the cheap-control linear-quadratic regulator (LQR) problem. Solve the control algebraic Ricatti equation

$$0 = PA + A^TP - PBB^TP + Q \tag{14}$$

and the control gain is obtained as $K_c = (1/\rho)B^TP$, where $Q = C^TC + qC^TC$ is the state weighting, ρ is the control weighting, and q is the recovery gain.

The LQG/LTR compensator K_{LQG} is then given by

$$K_{\mathrm{LQG}} = K_c(sI - A + BK_c + K_fC)^{-1}K_f. \tag{15}$$

By tuning the recovery gain ($q \to \infty$), the loop shape of the system loop transfer function $G(s)K_{\mathrm{LQG}}(s)$ will approach the target feedback loop constructed in Step 2. Since the designed plant model in this system is minimum phase, recovery of the target feedback loop can be arbitrarily good under the assumption of continuous linear systems. But in the design of a practical digital control system, q should be kept at a minimum value to satisfy the recovery requirement. Fig. 10 illustrates the recovery process by tuning the recovery gain q while the control weighting is set to be unity. The poles and zeros of K_{LQG} are shown in Table IV. The overall servo compensator $K(s)$ is given by $K(s) = G_a(s)K_{\mathrm{LQG}}(s)$.

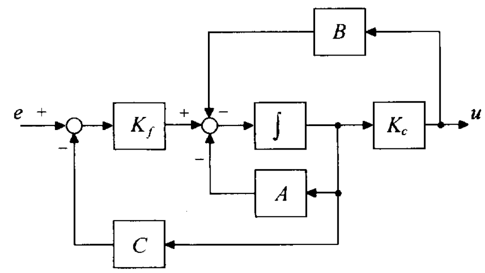

Fig. 9. Block diagram of the model-based compensator.

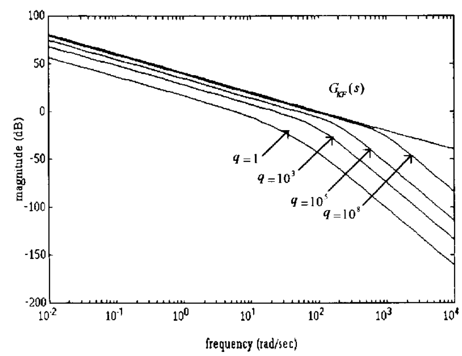

Fig. 10. Recovery process of the LQG/LTR compensator design.

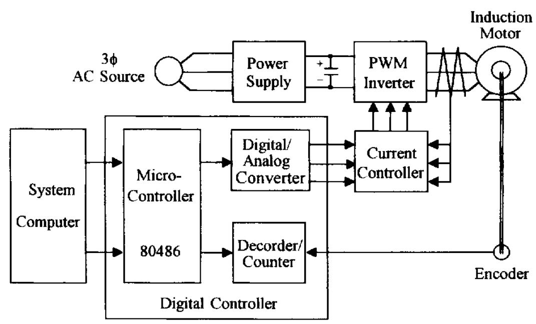

Fig. 11. Configuration of the microprocessor-based ac induction servo drive.

IV. SIMULATION AND EXPERIMENTAL RESULTS

The configuration of the proposed microprocessor-based ac induction servo drive system is shown in Fig. 11. This ac induction motor drive experimental system is composed of a power supply, a pulsewidth-modulated (PWM) voltage source inverter, a three-phase current controller, an ac induction motor, and the microprocessor-based digital controller.

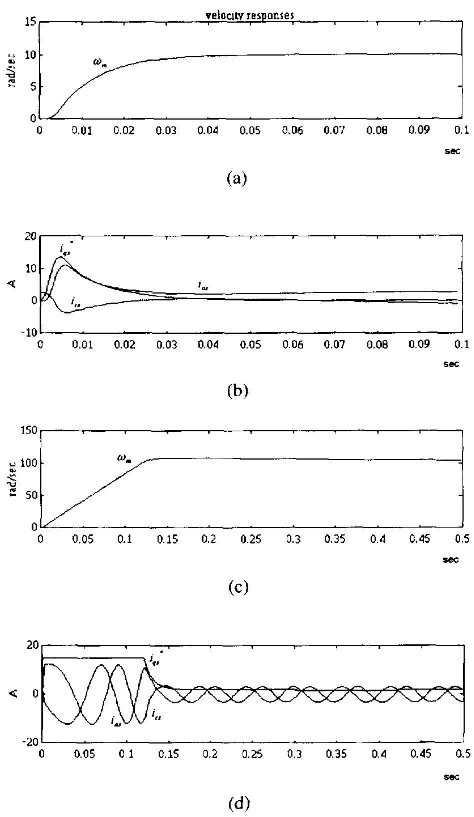

Fig. 12. Simulation results under step velocitychanges. Responses of 10 rad/sec step change: (a) Velocity. (b) Current signals. Responses of 100 rad/sec step change: (c) Velocity. (d) Current signals.

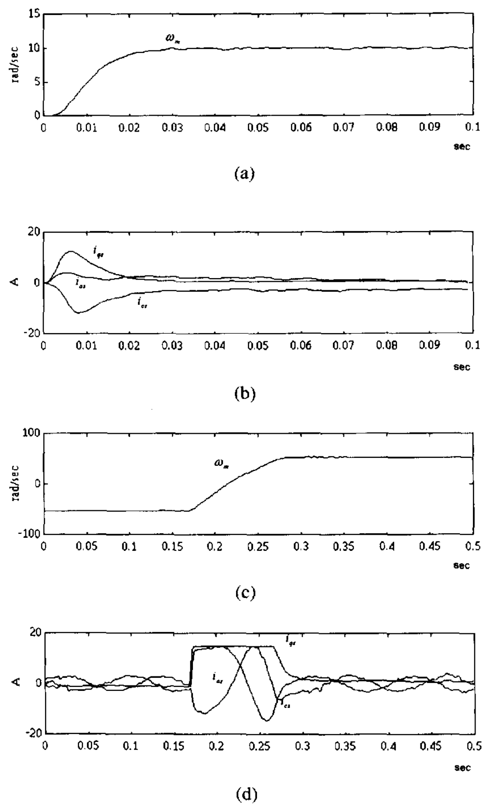

Fig. 13. Experimental results under step velocity changes. Responses of 10 rad/sec step change: (a) Velocity. (b) Current signals. Responses of velocity reversal: (c) Velocity. (d) Current signals.

The microprocessor-based digital controller is constructed to accomplish the ac induction servo drive control task which includes the servo loop compensation, field-oriented current decoupling control, feedback signal conditioning, and command interpretation. The microprocessor chosen for the digital controller is the Intel 80486 running at 33 MHz. This 32-bit microprocessor is equipped with a built-in numerical coprocessor, such that all mathematical operations are carried out using floating-point formats. The microprocessor is interfaced to the digital-to-analog converters, quadrature decoder-counter, and other peripherals via standard input-output channels. The outputs of the microprocessor-based digital controller are the three-phase stator current references. As the computing results of speed loop compensation and indirect vector control, the stator current references are converted into analog values by 12-bit digital-to-analog converters Am6012. The only feedback signal to the digital controller is the motor shaft angular position. The motor shaft position is measured by an optical encoder which generates 2000 pulses per revolution. The quadrature decoder-counter HCTL2000 is used to increase the pulses to 8000 via using a multiply-by-four logic circuit and present the shaft position digital value via a 12-bit up-down counter. The motor angular velocity is then obtained by using the measured motor shaft position and a backward difference interpolation.

To implement the speed-loop control algorithm, discretization of the continuous transfer function is required. The sampling rate is set at 1 kHz to convert the continuous LQG/LTR controller to its digital equivalent. The digital equivalent of the LQG/LTR compensator transfer function is developed using the bilinear transformation with frequency prewarping. The final form of the digital equivalent transfer function of the LQG/LTR servo controller is

$$K(z) = 0.1553 \frac{(1+z^{-1})(1+0.0017z^{-1}-0.9983z^{-2})}{(1-z^{-1})(1-0.8423z^{-1}+0.2987z^{-2})}. \tag{16}$$

By using the timer on the digital controller it is possible to measure the computation time required for one execution of the induction motor velocity control loop. The execution time of the LQG/LTR servo control algorithm takes 164 μsec, the indirect vector control 308 μsec and the input-output device processing 80 μsec which make the total computation time of the induction motor velocity servo control action up to 552 μsec, approximately 55% of the sampling period.

The induction motor is driven by a current-controlled PWM voltage source inverter. Each phase of the induction motor stator current is measured by a Hall-effect sensor and compared independently with its corresponding reference command which is generated by the microprocessor-based digital

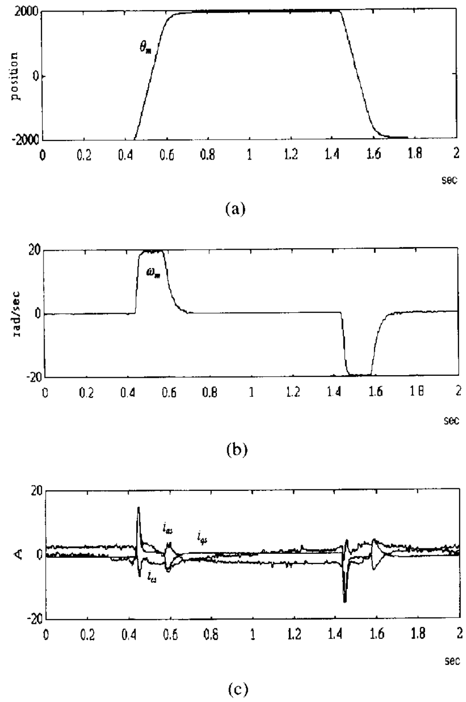

Fig. 14. Experimental results under step position changes: (a) Responses of the shaft position. (b) Velocity. (c) Current signals.

controller. The current error of each phase is manipulated by a PI-type current loop compensator and then the PWM signal generator. The outputs of the PWM signal generator are pulse signals which directly determines the power device firing commands of the inverter. Power MOSFET's operating at 20 kHz are used as switching devices to achieve the high performance of the current-controlled inverter.

The simulation and experimental results can validate the proposed control scheme and the theoretical development. The parameters of the ac induction servo motor used in the experimental system are listed in Table V.

Fig. 12 and Fig. 13 show the simulation and experimental results of the dynamic responses of the fully digitized LQG/LTR controlled ac induction servo drive under step velocity changes. The dynamic signals shown in figures are the rotor velocity ω_m, torque-producing current command i_{qs}^*, stator phase current i_{as} and i_{cs} of the induction servo motor. The experimental system is operated with a uniform sampling rate such that the signals are sampled every 1 msec. Figs. 12(a) and (c) show the simulated velocity responses of 10 rad/sec and 100 rad/sec step changes respectively. Figs. 12(b) and (d) give the corresponding current signals during the same period of operation. It should be noted that the torque-producing current command is limited within 15 A to prevent the over-current operation of the inverter power devices and the flux-producing current command is kept as a constant value while the motor operates within the constant torque region. Figs. 13(a) and (b) show the measured speed and current responses of 10 rad/sec step change. Comparing the

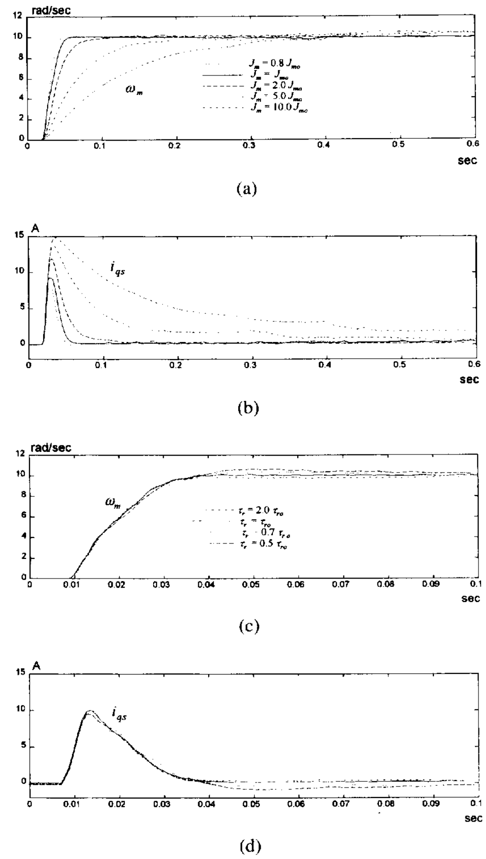

Fig. 15. Experimental results with load and parameter variations. Responses with changing shaft inertia: (a) Velocity. (b) Current signals. Responses with changing rotor time constant: (c) Velocity. (d) Current signals.

TABLE V
PARAMETERS OF THE AC INDUCTION MOTOR

Type: 3-phase, Y-connection, 2-pole, 800 W	
$R_s = 1.1\Omega$	$L_s = 0.145H$
$R_r = 1.3\Omega$	$L_r = 0.145H$
	$L_m = 0.136H$

waveforms of Figs. 12(a) and (b) and Figs. 13(a) and (b), the similarity of the simulation and experimental results confirms the development of the mathematical model and the servo controller. Figs. 13(c) and (d) show recorded transients of the velocity reversal operation from −50 to 50 rad/sec. The rapid response is exemplified by the fact that the motor completes the velocity reversal after turning only one revolution. Fig. 14 shows the step position responses while the position control loop and a P-type position controller are appended. The pulse count is used to present the motor shaft angular position shown in Fig. 14(a) and 4000 pulses step change makes a half shaft revolution. Figs. 14(b) and (c) show the corresponding velocity and current dynamic signals of the same operation period. The fast dynamic responses of the rotor velocity and torque current show the effectiveness of the software-based current decoupling control scheme and the LQG/LTR servo controller. Fig. 15 presents the speed step responses with load and parameter variations. Figs. 15(a) and (b) show the speed and torque producing current responses with changes in the shaft load. As shown in the figure, the shaft inertia has been changed from 0.8 to 10 times of the nominal inertia value $J_{mo} = 0.0075$ Kg-m^2. These results show that the servo controller successfully stabilizes the servo drive system against large load variations. The rotor time constant is chosen for the parameter varying test not only because it varies with temperature and magnetic saturation but also it influences the decupling control, and thus the accuracy of the equivalent model. The value of the rotor time constant is nominal for Figs. 15(a) and (b); Figs. 15(c) and (d) show the effect of varying the rotor time constant while the load value is nominal. With $\tau_{ro} = 0.112$ sec represents the nominal value of the rotor time constant, the parameter varying test is done by changing the rotor constant value instrumented in the decoupling controller from 0.5 to 2.0 times of the nominal value. Fast responses are still obtained, but the LQG/LTR control does not yield performance independent of the rotor time constant changes due to the loss of decoupling control.

V. Conclusion

In the design and implementation of an ac induction servo drive, the feedforward indirect field orientation has been used to achieve the fast response current decoupling control action and form a equivalent nominal plant model. The LQG/LTR methodology has been used to design the servo controller that shapes the speed loop transfer function to satisfy the performance and stability-robustness specifications. A specification-oriented systematic procedure has been proposed and presented.

An experimental prototype system based on a high-performance microprocessor implementation has been constructed to evaluate the proposed control scheme. Laboratory testing with consideration of motor parameter and load variations have been carried out. Experimental results have shown the effectiveness of the proposed control scheme and the feasibility of the LQG/LTR methodology in high-performance ac induction servo drive design.

References

[1] F. Blaschke, "The principle of field orientation as applied to the new TRANSVECTOR closed loop control system for rotating field machines," *Siemens Rev.*, vol. 34, pp. 217–220, 1972.

[2] R. Gabriel, W. Leonhard, and C. J. Nordby, "Field-oriented control of a standard ac motor using microprocessors," *IEEE Trans. Ind. Applicat.*, vol. 16, pp. 186–192, Mar./Apr. 1980.

[3] F. Harashima, S. Kondo, K. Ohnishi, M. Kajita, and M. Susono, "Multimicroprocessor-based control system for quick response induction motor drive," *IEEE Trans. Ind. Applicat.*, vol. 21, pp. 602–609, May/June 1985.

[4] E. J. Davison and A. Goldenberg, "Robust control of a general servomechanism problem: the servo compensator," *Automatica*, vol. 11, pp. 461–471, 1975.

[5] J. C. Doyle and G. Stein, "Multivariable feedback design: concept for a classical/modern synthesis," *IEEE Trans. Automat. Contr.*, vol. 26, pp. 4–16, Feb. 1981.

[6] M. A. Johnson and M. J. Grimble, "Recent trends in linear optimal quadratic multivariable control system design," *IEE Proc.*, vol. 134, pp. 53–71, Jan. 1987.

[7] G. Stein and M. Athans, "The LQG/LTR procedure for multivariable feedback control design," *IEEE Trans. Automat. Contr.*, vol. 32, pp. 105–106, Feb. 1987.

[8] D. B. Ridgely, S. S. Banda, T. E. McQuade, and P. J. Lynch, "Linear-quadratic-Gaussian with loop-transfer-recovery methodology for an unmanned aircraft," *J. Guidance*, vol. 10, no. 1, pp. 82–89, Jan. 1987.

[9] H. Hanselmann and A. Engelke, "LQG-control of a highly resonant disk drive head positioning actuator," *IEEE Trans. Ind. Electron.*, vol. 35, pp. 100–104, Feb. 1988.

[10] Z. K. Wu, "Feed forward field orientation control of an induction motor using a PWM voltage source inverter and standardized single-board computers," *IEEE Trans. Ind. Electron.*, vol. 35, pp. 75–79, Feb. 1988.

[11] IEEE Std. 112–1984, *IEEE Standard Test Procedure for Polyphase Induction Motors and Generators*. New York: IEEE Press, 1984.

[12] J. Holtz and T. Thimm, "Identification of the machine parameters in a vector controlled induction motor drive system," *IEEE Trans. Ind. Applicat.*, vol. 27, pp. 1111–1118, Nov./Dec. 1991.

Ying-Yu Tzou (S'81-M'88) was born in Taiwan, Republic of China, on February 13, 1956. He received the B.S. and M.S. degrees in control engineering from the National Chiao Tung University, and the Ph.D. degree in electrical engineering from the Institute of Electronics Engineering of National Chiao Tung University in 1978, 1983, and 1987, respectively.

During 1980–1981, he was with the Electronic Research and Service Organization (ERSO) of Industry Technology Research Institute (ITRI) as a design engineer in the control system department for Factory Automation. During 1983–1986 he was with Microtek Automation, Inc., as a project manager for the development a Computer Numerical Controller (CNC) for machine tools. He has been an Associate Professor in the Department of Control Engineering of National Chiao Tung University since August 1987.

His special areas of interest are DSP-based power electronics systems, motion control system, servo drives, parallel processing and control, and fuzzy control systems.

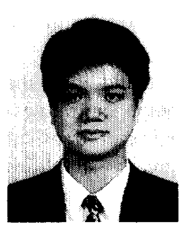

Hsiang-Jui Wu was born in Taiwan, Republic of China, on October 7, 1964. He received the B.S. and M.S. degrees in control engineering from the National Chiao Tung University, Taiwan, Republic of China, in 1986 and 1988, respectively. He received the Ph.D. degree in electrical engineering from the Institute of Electronics Engineering of the same University in 1994.

He has been with the ViewSonic International Co., Taiwan, as a R&D specialist since September 1994.

Among his research interests are power electronics, ac and dc servo drives, digital signal processing, and microprocessor applications in control.